applied sciences

MDPI

Article

Advanced Dynamic Thermal Vibration of Laminated FGM Plates with Simply Homogeneous Equation by Using TSDT and Nonlinear Varied Shear Coefficient

Chih-Chiang Hong

Department of Mechanical Engineering, Hsiuping University of Science and Technology, Taichung 412-406, Taiwan; cchong@mail.hust.edu.tw

Abstract: The effects of advanced nonlinear varied shear coefficient and third-order shear deformation theory (TSDT) on the dynamic responses of thick functionally graded material (FGM) plates under thermal vibration are investigated. The nonlinear coefficient of the displacement field of TSDT is used to obtain the expression of advanced varied shear coefficient for the thick FGM plates. The dynamic displacements, shear rotations and stresses in numerical results under sinusoidal applied heat loads are obtained and investigated. Two parametric effects of environment temperature and FGM power law index on the dynamic responses of thermal stress and center deflection of thick FGM plates are also investigated. The transient responses of center deflection are found for the cases of simply homogeneous equation and fully homogeneous equation. Also, the transient responses of center deflection are found for cases of nonlinear and linear varied-modified coefficient of shear correction.

Keywords: advanced; nonlinear; shear correction; TSDT; dynamic responses; thick FGM plates

Citation: Hong, C.-C. Advanced Dynamic Thermal Vibration of Laminated FGM Plates with Simply Homogeneous Equation by Using TSDT and Nonlinear Varied Shear Coefficient. *Appl. Sci.* **2022**, *12*, 11776. https://doi.org/10.3390/app122211776

Academic Editor: Victor Franco Correia

Received: 31 October 2022
Accepted: 18 November 2022
Published: 19 November 2022

1. Introduction

There are some investigations of shear deformation effects in composited plates. In 2020, Zenkour and El-Shahrany [1] used various displacement theories, e.g., third-order shear deformation theory (TSDT), first-order shear deformation theory (FSDT), etc., to study laminated magnetostrictive plates; in their research, the numerical dynamic results of vibration suppression are presented. There are some dynamical investigations of thermal vibrations in the temperature environment. In 2020, Wu et al. [2] used an experimental test for hypersonic vehicles to investigate the vibration of lightweight ceramic insulating material in extremely thermal conditions. In 2020, Shariyat and Mohammadjani [3] applied a three-dimensional (3D) nonlinear variable thermos-viscoelastic numerical theory to investigate the dynamic stress and time response of vibration in thick functionally graded material (FGM) rotating annular plates undergoing temperature rises. In 2020, Fan et al. [4] presented the numerical analysis of a 3D integrated package to investigate the fatigue of through-silicon-via copper (TSV-Cu) structures under thermal and vibration coupled loads. In 2019, Su et al. [5] used FSDT in a numerical approach to investigate the flutter and vibration of stiffened FGM plates under different temperature conditions. In 2019, Fang et al. [6] used two versions of Euler–Bernoulli beam theory (EBT) and Timoshenko beam theory (TBT) in a numerical approach to study the thermal vibration behaviors of rotating FGM micro-beams. In 2016, Duc et al. [7] used FSDT in a numerical approach to calculate the dynamic and vibration for piezoelectric FGM plates under different temperature conditions. In 2006, Huang and Shen [8] used higher-order shear deformation theory (HSDT) in a numerical approach to investigate the time response of piezoelectric FGM plates under different temperature conditions. In 2004, Huang and Shen [9] used HSDT in a numerical approach to investigate the time response of FGM plates under different temperature conditions.

The generalized differential quadrature (GDQ) method has been applied for FGM plates. In 2019, Hong [10] studied the dynamic responses of thick FGM plates by using the TSDT effect and fully homogeneous equation under different temperature conditions. The simply modified factor of shear correction was used without considering the nonlinear terms of TSDT. In 2014, Hong [11] studied the dynamic responses of Terfenol-D FGM plates by considering the FSDT effect and the simply modified factor of shear correction under different temperature conditions. In 2012, Hong [12] presented the dynamic responses for Terfenol-D FGM plates by using the FSDT effect and constant value of shear correction equal to 5/6 under rapid heating. It is interesting to further study the dynamic responses of stresses and deflection in the TSDT approach of GDQ computations, and the advanced nonlinear varied-modified coefficient of shear correction for thick FGM plates under different temperature condition. The parametric effects of temperature and power law index of FGM on the dynamic responses of stress and deflection are investigated for thick FGM plates.

This paper will proceed as follows. Firstly, the advanced nonlinear varied-modified coefficient of shear correction including the coefficient term z^3 of TSDT is presented. Secondly, the dynamic responses of stresses and deflection in GDQ computation are presented. Finally, the parametric effects of temperature and power law index of FGM on the dynamic responses of stress and deflection are presented.

2. Formulation Procedures

The two constituent materials of the FGM plate (e.g., FGM material 1 and FGM material 2) are shown in Figure 1. Along the axes of x and y, the lengths are a and b, respectively. The thickness of FGM material 1 is h_1, the thickness of FGM material 2 is h_2 and the total thickness of the FGM plates is h^* in the direction of z in the Cartesian system. Young's modulus of thick FGM plates in power law function are used in the standard form of index R_n under environment temperature T. The other properties are assumed in the average values of forms. The individual properties P_i of the constituent material of the FGMs are functions of T which can be obtained. The time dependent of displacements u and v of the thick FGM plates can be assumed in the nonlinear forms with respect to z direction by using the coefficient $c_1 c_1$ term of TSDT equations [13] as follows,

$$\begin{bmatrix} u \\ v \\ w \end{bmatrix} = \begin{bmatrix} u^0(x,y,t) \\ v^0(x,y,t) \\ w(x,y,t) \end{bmatrix} + z \begin{bmatrix} \psi_x(x,y,t) \\ \psi_y(x,y,t) \\ 0 \end{bmatrix} - c_1 z^3 \begin{bmatrix} \psi_x + \frac{\partial_w}{\partial_x} \\ \psi_y + \frac{\partial_w}{\partial_y} \\ 0 \end{bmatrix}, \tag{1}$$

in which t is time. Coefficient for $c_1 = 4/\left(3h^{*2}\right)$ is given in the TSDT approach, and u^0, v^0 and w are the displacements in the x, y and z axes of the middle-plane of the thick FGM plates, respectively. ψ_x and ψ_y are the shear rotations in the x and y directions.

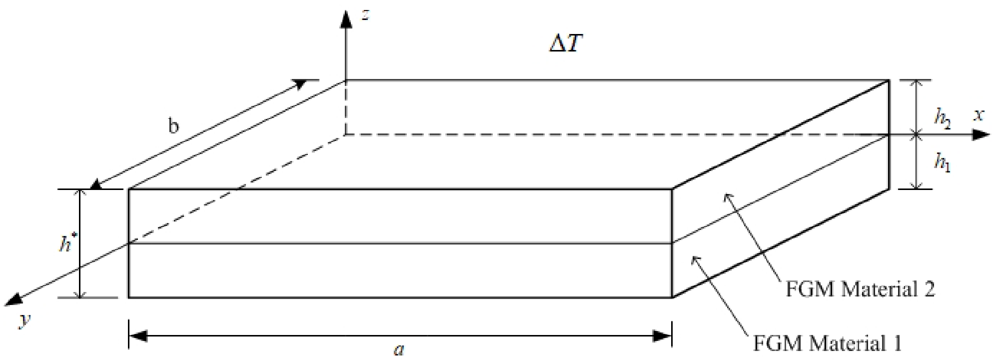

Figure 1. Thick FGM plate under sinusoidal applied heat loads.

The stresses in normal direction (σ_x and σ_y) and in the shear direction (σ_{xy}, σ_{yz} and σ_{xz}) for the thick FGM plate under temperature difference ΔT can be obtained and expressed in terms of the products of stiffness and strains with thermal coefficients α_x, α_y and α_{xy}. The parameter ΔT between the thick FGM plate and the curing environment area can be obtained in linear form with z, also in sinusoidal form with x, y and t that can be expressed by Hong as follows [10],

$$\Delta T = \left[\frac{z}{h^*}\overline{T}_1 sin\left(\frac{\pi x}{a}\right) sin\left(\frac{\pi y}{b}\right)\right] sin(\gamma t) \tag{2}$$

in which γ is the frequency of applied heat flux, $\overline{T}_1$ is the temperature amplitude of applied heat loads.

The dynamic equations of motion with nonlinear TSDT for a thick FGM plate can be obtained by assuming that the first partial differentiation in displacements and shear rotations with respect to z are going to zero in the strain-displacement relations [14]. The dynamic equilibrium differential equations with nonlinear TSDT of thick FGM plates could be obtained by Hong [10] with the following integrals for the stiffness $\overline{Q}_{i^s j^s}$ and $\overline{Q}_{i^* j^*}$ in the z direction, respectively,

$$(A_{i^s j^s}, B_{i^s j^s}, D_{i^s j^s}, E_{i^s j^s}, F_{i^s j^s}, H_{i^s j^s}) = \int_{\frac{-h^*}{2}}^{\frac{h^*}{2}} \overline{Q}_{i^s j^s}(1, z, z^2, z^3, z^4, z^6)dz,\ (i^s, j^s = 1, 2, 6), \tag{3a}$$

$$(A_{i^* j^*}, B_{i^* j^*}, D_{i^* j^*}, E_{i^* j^*}, F_{i^* j^*}, H_{i^* j^*}) = \int_{\frac{-h^*}{2}}^{\frac{h^*}{2}} k_\alpha \overline{Q}_{i^* j^*}(1, z, z^2, z^3, z^4, z^5)dz,\ (i^*, j^* = 4, 5), \tag{3b}$$

where k_α is the advanced nonlinear varied-modified coefficient of shear correction.

In the advanced nonlinear varied k_α expression including the $c_1 c_1$ terms for the thick FGM plates in terms of Young's modulus E_1 and E_2 in constituent material 1 and 2, respectively, can be obtained as follows,

$$k_\alpha = \frac{1}{h^*}\frac{FGMZSV}{FGMZIV} \tag{4}$$

where

$FGMZSV = (FGMZS - c_1 FGMZSN)^2$,

$FGMZIV = FGMZI - 2c_1 FGMZIV1 + {c_1}^2 FGMZIV2$,

$$FGMZS = \frac{E_2 - E_1}{h^{*R_n}}\left[\frac{\left(\frac{h^*}{2} + \frac{h^*}{2}\right)^{R_n+3}}{R_n + 3} - \frac{h^*\left(\frac{h^*}{2} + \frac{h^*}{2}\right)^{R_n+2}}{(R_n + 2)} + \frac{h^{*2}\left(\frac{h^*}{2} + \frac{h^*}{2}\right)^{R_n+1}}{4(R_n + 1)}\right] + E_1\left(\frac{h^{*3}}{24} + \frac{h^{*3}}{24}\right)$$

$$\begin{aligned} FGMZSN = {} & \frac{E_2 - E_1}{h^{*R_n}}\left[\frac{\left(\frac{h^*}{2} + \frac{h^*}{2}\right)^{R_n+5}}{R_n+5} - \frac{2h^*\left(\frac{h^*}{2} + \frac{h^*}{2}\right)^{R_n+4}}{R_n+4} + \frac{3h^{*2}\left(\frac{h^*}{2} + \frac{h^*}{2}\right)^{R_n+3}}{2(R_n+3)}\right. \\ & \left. - \frac{h^{*3}\left(\frac{h^*}{2} + \frac{h^*}{2}\right)^{R_n+2}}{2(R_n+2)} + \frac{h^{*4}\left(\frac{h^*}{2} + \frac{h^*}{2}\right)^{R_n+1}}{16(R_n+1)}\right] + E_1\left(\frac{h^{*5}}{160} + \frac{h^{*5}}{160}\right) \end{aligned}$$

$$\begin{aligned} FGMZI = {} & (E_2 - E_1)^2 h^{*5}\left[\frac{1}{(R_n+2)^2(2R_n+5)} - \frac{1}{(R_n+1)(R_n+2)(2R_n+4)} + \frac{1}{4(R_n+1)^2(2R_n+3)}\right] \\ & + 2(E_2 - E_1)h^{*5}\left\{\frac{E_1}{2(R_n+2)}\left[\frac{1}{R_n+5} - \frac{1}{R_n+4} + \frac{1}{4(R_n+3)}\right]\right. \\ & \left. - \frac{E_1}{4(R_n+1)}\left[\frac{1}{R_n+4} - \frac{1}{R_n+3} + \frac{1}{4(R_n+2)}\right]\right\} \\ & - \frac{2E_1 h^{*5}}{8}\left\{(E_2 - E_1)\left[\frac{1}{(R_n+2)(R_n+3)} - \frac{1}{2(R_n+1)(R_n+2)}\right] + \frac{E_1}{24}\right\} \\ & + {E_1}^2 h^{*5}\left(\frac{1}{320} + \frac{1}{64}\right) \end{aligned}$$

$$
\begin{aligned}
FGMZIV1 = (E_2 - E_1)^2 h^{*7} \Big[& \tfrac{1}{(R_n+2)(R_n+4)(2R_n+7)} - \tfrac{3}{2(R_n+2)(R_n+3)(2R_n+6)} \\
& + \tfrac{3}{4(R_n+2)^2(2R_n+5)} - \tfrac{1}{2(R_n+1)(R_n+2)(2R_n+4)} \\
& - \tfrac{1}{2(R_n+1)(R_n+4)(2R_n+4)} + \tfrac{3}{4(R_n+1)(R_n+3)(2R_n+5)} \\
& + \tfrac{1}{16(R_n+1)^2(2R_n+3)} \Big] \\
& + E_1(E_2 - E_1)h^{*7} \Big[\tfrac{1}{2(R_n+4)} \left(\tfrac{1}{R_n+7} - \tfrac{1}{R_n+6} + \tfrac{1}{4(R_n+5)} \right) \\
& - \tfrac{1}{8(R_n+4)(R_n+5)} - \tfrac{3}{4(R_n+3)} \left(\tfrac{1}{R_n+6} - \tfrac{1}{R_n+5} + \tfrac{1}{4(R_n+4)} \right) \\
& + \tfrac{3}{16(R_n+3)(R_n+4)} + \tfrac{3}{8(R_n+2)} \left(\tfrac{1}{R_n+5} - \tfrac{1}{R_n+4} + \tfrac{1}{4(R_n+3)} \right) \\
& - \tfrac{7}{64(R_n+2)(R_n+3)} - \tfrac{1}{16(R_n+1)} \left(\tfrac{1}{R_n+4} - \tfrac{1}{R_n+3} + \tfrac{1}{4(R_n+2)} \right) \\
& + \tfrac{3}{128(R_n+1)(R_n+2)} \\
& + \tfrac{1}{4(R_n+2)} \left(\tfrac{1}{R_n+7} - \tfrac{2}{R_n+6} + \tfrac{3}{2(R_n+5)} - \tfrac{1}{2(R_n+4)} + \tfrac{1}{16(R_n+3)} \right) \\
& - \tfrac{1}{8(R_n+1)} \left(\tfrac{1}{R_n+6} - \tfrac{2}{R_n+5} + \tfrac{3}{2(R_n+4)} - \tfrac{1}{2(R_n+3)} + \tfrac{1}{16(R_n+2)} \right) \Big] \\
& + {E_1}^2 h^{*7} \left(\tfrac{1}{3584} - \tfrac{1}{2560} - \tfrac{1}{1536} + \tfrac{1}{512} \right)
\end{aligned}
$$

$$
\begin{aligned}
FGMZIV2 = (E_2 - E_1)^2 h^{*9} \Big[& \tfrac{1}{(R_n+4)^2(2R_n+9)} - \tfrac{9}{4(R_n+3)^2(2R_n+7)} \\
& + \tfrac{9}{16(R_n+2)^2(2R_n+5)} - \tfrac{1}{64(R_n+1)^2(2R_n+3)} \\
& - \tfrac{3}{(R_n+3)(R_n+4)(2R_n+8)} + \tfrac{3}{2(R_n+2)(R_n+4)(2R_n+7)} \\
& - \tfrac{1}{4(R_n+1)(R_n+4)(2R_n+6)} - \tfrac{9}{4(R_n+2)(R_n+3)(2R_n+6)} \\
& + \tfrac{3}{8(R_n+1)(R_n+3)(2R_n+5)} - \tfrac{3}{16(R_n+1)(R_n+2)(2R_n+4)} \Big] \\
+ 2(E_2 - E_1)E_1 h^{*9} \Big[& \tfrac{1}{4(R_n+4)} \left(\tfrac{1}{R_n+9} - \tfrac{2}{R_n+8} + \tfrac{3}{2(R_n+7)} - \tfrac{1}{2(R_n+6)} + \tfrac{1}{16(R_n+5)} \right) \\
& - \tfrac{3}{8(R_n+3)} \left(\tfrac{1}{R_n+8} - \tfrac{2}{R_n+7} + \tfrac{3}{2(R_n+6)} - \tfrac{1}{2(R_n+5)} + \tfrac{1}{16(R_n+4)} \right) \\
& + \tfrac{3}{16(R_n+2)} \left(\tfrac{1}{R_n+7} - \tfrac{2}{R_n+6} + \tfrac{3}{2(R_n+5)} - \tfrac{1}{2(R_n+4)} + \tfrac{1}{16(R_n+3)} \right) \\
& - \tfrac{1}{32(R_n+1)} \left(\tfrac{1}{R_n+6} - \tfrac{2}{R_n+5} + \tfrac{3}{2(R_n+4)} - \tfrac{1}{2(R_n+3)} + \tfrac{1}{16(R_n+2)} \right) \\
& - \tfrac{1}{64} \Big(\tfrac{1}{(R_n+4)(R_n+5)} - \tfrac{3}{2(R_n+3)(R_n+4)} + \tfrac{3}{4(R_n+2)(R_n+3)} \\
& - \tfrac{1}{8(R_n+1)(R_n+2)} \Big) \Big] + {E_1}^2 h^{*9} \left(\tfrac{1}{36864} - \tfrac{1}{10240} + \tfrac{1}{256} \right)
\end{aligned}
$$

The values of advanced nonlinear k_α are usually functions of c_1, R_n and T, but is independent to the value of h^*. The GDQ numerical method is used in the computation for the derivative of a smooth function at a coordinate of an arbitrary grid point (x_i, y_j), in which subscripts $i = 1, 2, \ldots, N$ and $j = 1, 2, \ldots, M$ in a domain [11,15–17]. The clarification of k_α expression in Equation (4) can be presented in more detail and is referred to in 2022 by Hong [18]. The non-dimensional parameters (X, Y, U, V and W) are used in the GDQ approaches under no in-plane distributed forces and no external pressure load ($q = 0$) as follows,

$$X = x/a,\ Y = y/b,\ U = u^0/a,\ V = v^0/b,\ W = 10h^* w/(\alpha_x \overline{T} a^2). \tag{5}$$

The displacement and shear rotations are assumed in time sinusoidal form of vibrations and expressed in the following,

$$\begin{bmatrix} u^0(x,y,t) \\ v^0(x,y,t) \\ w(x,y,t) \\ \psi_x(x,y,t) \\ \psi_y(x,y,t) \end{bmatrix} = \begin{bmatrix} u^0(x,y) \\ v^0(x,y) \\ w(x,y) \\ \psi_x(x,y) \\ \psi_y(x,y) \end{bmatrix} \sin(\omega_{mn} t), \quad (6)$$

in which ω_{mn} is the natural frequency of the thick FGM plate with subscript mode shape numbers m and n. Boundary equations of displacements and shear rotations with amplitudes: a_{mn}, b_{mn}, c_{mn}, d_{mn}, and e_{mn} for four-sided simply supported plates are given explicitly in Appendix A.

3. Some Numerical Results and Discussions

The coordinates x_i and y_j in the computational domain for the grid points N and M of the thick FGM plates are implemented to calculate the displacements and shear rotations of GDQ results under applied heat loads and listed as follows.

$$x_i = 0.5[1 - \cos(\frac{i-1}{N-1}\pi)]a, i = 1, 2, \ldots, N \quad (7a)$$

$$y_j = 0.5[1 - \cos(\frac{j-1}{M-1}\pi)]b, j = 1, 2, \ldots, M \quad (7b)$$

Also, the dynamic inter-laminar stresses in the constituent layer could be calculated when the displacements and shear rotations are obtained for the given ω_{mn} and time. The simply homogeneous equation can be obtained by assuming that matrix elements in (row, column) with (1,3)–(1,5); (2,3)–(2,5); (3,1)–(3,2); (4,1)–(4,2) and (5,1)–(5,2) are neglected in the coefficient matrix of fully homogeneous equation in 2019 by Hong [10]. The determinant of the coefficient matrix in a simply homogeneous equation going to zero could be obtained in the simply five degree polynomial equation, thus the ω_{mn} values could be calculate.

3.1. Dynamic Convergence Study

The FGM constituent material 1 located at lower position is stainless steel (SUS304); the FGM constituent material 2 located at upper position is silicon nitride (Si_3N_4) used with h_1 = h_2 under applied heat temperature $\overline{T_1}$ and T. The convergence of center displacement amplitude $w(a/2, b/2)$ (unit mm) are studied for the thick FGM plates at t = 6 s with $a/b = 1$, c_1 = 0.925925/mm^2, h_1 = h_2 = 0.6 mm, T = 100 K and $\overline{T_1}$ = 100 K. The calculated values of $w(a/2, b/2)$ for a/h^* = 10 with applied heat flux γ = 0.2618004/s and a/h^* = 5 with γ = 0.2618019/s, respectively, are obtained and listed in Table 1 by using the advanced nonlinear varied k_α and ω_{11} under three values of R_n. For a/h^* = 10, the values are calculated and used in case 1: ω_{11} = 0.059249/s and R_n = 0.5; in case 2: ω_{11} = 0.061595/s and R_n = 1; in case 3: ω_{11} = 0.064255/s and R_n = 2. For a/h^* = 5, the values are calculated and used in case 1: ω_{11} = 0.018034/s and R_n = 0.5; in case 2: ω_{11} = 0.032166/s and R_n = 1; in case 3: ω_{11} = 0.032121/s and R_n = 2. The error accuracy of the amplitude $w(a/2, b/2)$ is 2.702918E-05 for R_n = 0.5 and a/h^* = 10. The grid point 13 $\times$ 13 could be considered in enough grid numbers to provide the acceptable convergence for the amplitude $w(a/2, b/2)$ and used continuously in the next time response of calculations. The advanced nonlinear k_α values for $a/b = 1$ under T = 100 K are shown in Table 2, they are typically varied with the three parameters: c_1, R_n and T. The typical ω_{mn} (unit 1/s) vs. mode shapes m and n (from 1 to 9) of the vibrating plate are reported in Table A1 and listed in Appendix A.

Table 1. Dynamic convergence of $w(a/2, b/2)$ considering advanced nonlinear k_α.

a/h^*	GDQ Method	$w(a/2,b/2)$ (Unit mm) at t = 6 s		
	$N \times M$	R_n=0.5	R_n=1	R_n=2
10	7 × 7	-5.289845×10^{-7}	-1.307268×10^{-6}	-4.786723×10^{-6}
	9×9	-5.290359×10^{-7}	-1.307458×10^{-6}	-4.788880×10^{-6}
	11 × 11	-5.290720×10^{-7}	-1.307463×10^{-6}	-4.788953×10^{-6}
	13 × 13	-5.290577×10^{-7}	-1.307423×10^{-6}	-4.788916×10^{-6}
5	7 × 7	-1.058373×10^{-4}	-5.050262×10^{-5}	-1.163284×10^{-4}
	9 × 9	-1.053382×10^{-4}	-5.060298×10^{-5}	-1.163351×10^{-4}
	11 × 11	-1.053358×10^{-4}	-5.047129×10^{-5}	-1.163347×10^{-4}
	13 × 13	-1.057038×10^{-4}	-5.047105×10^{-5}	-1.163352×10^{-4}

Table 2. Nonlinear varied k_α vs. c_1 and R_n under T = 100 K.

c_1 (1/mm^2)	h^* (mm)	k_α						
		R_n=0.1	R_n=0.2	R_n=0.5	R_n=1	R_n=2	R_n=5	R_n=10
92.592598	0.12	−0.448521	−0.456089	−0.539418	−0.922718	9.852672	0.682434	0.491249
0.925925	1.2	−0.448522	−0.456090	−0.539419	−0.922719	9.852635	0.682434	0.491249
0.231481	2.4	−0.448522	−0.456089	−0.539419	−0.922719	9.852635	0.682434	0.491249
0.037037	6	−0.448522	−0.456089	−0.539418	−0.922718	9.852679	0.682434	0.491249
0.009259	12	−0.448522	−0.456089	−0.539418	−0.922718	9.852675	0.682434	0.491249
0	1.2	0.899095	0.957858	1.091129	1.200860	1.232039	1.126363	1.021824

3.2. Time Responses of Deflection and Stress

In Figures 2–7, the horizontal and vertical axes have units, e.g., in Figure 2, the unit for $w(a/2, b/2)$ in the vertical axis is "mm", and the unit for t in the horizontal axis is "sec". In Figure 3, the unit for σ_x in the vertical axis is "GPa", the unit for t in the horizontal axis is "sec". In Figure 4, the unit for $w(a/2, b/2)$ in the vertical axis is "mm", the unit for T in the horizontal axis is "K". In Figure 5, the unit for σ_x in the vertical axis is "GPa", the unit for T in the horizontal axis is "K". The time responses of deflection and stress are computed with the γ value decreasing from γ = 15.707964/s at t = 0.1 s to γ = 0.523601/s at t = 3.0 s. Figure 2 shows the time response of $w(a/2, b/2)$ (unit mm) for a/h^* = 5 and 10, respectively, with c_1 = 0.925925/mm^2, $R_n = 1$, T = 600 K and $\overline{T_1}$ = 100 K. The maximum absolute value of $w(a/2, b/2)$ is 0.006138 mm at = 0.1 s found for a/h^* = 5 with advanced k_α = −3.535402 and γ = 15.707964/s. The time responses of $w(a/2, b/2)$ are converging at around 0.0 for a/h^* = 5 and 10.

Typically the stress values vary through the plate thickness by considering the effect of advanced nonlinear varied k_α values. Figure 3a,b show the time responses of the dominated stresses σ_x (unit GPa) at the center position of lower surface $z = -0.5h^*$ as the analyses of deflection case in Figure 2 for R_n = 1, a/h^* = 5 and 10, respectively. The absolute value of maximum stresses σ_x is -9.685218×10^{-4} GPa found at t = 2.4 s for thick a/h^* = 5. The time responses of stresses σ_x are oscillating around $-$ 9.50 × 10^{-4} GPa for a/h^* = 5 and around -9.035×10^{-4} GPa for a/h^* = 10.

3.3. Deflection and Stress vs. T and R_n

Figure 4 shows $w(a/2, b/2)$ (unit mm) vs. T (unit K) for R_n (from 0.1 to 10) at t = 2.4 s with γ = 0.654498/s, advanced nonlinear k_α, c_1 = 0.925925/mm^2, $\overline{T_1}$ = 100 K, a/h^* = 5 and 10, respectively. Figure 4a shows the R_n curves in a/h^* = 5; the absolute value of maximum $w(a/2, b/2)$ is −0.003227 mm found at T = 600 K for R_n = 2. The absolute values of $w(a/2, b/2)$ for R_n = 0.5, 1 and 2 can proceed in higher T = 1000 K of temperature condition. The center deflection amplitude values are almost keep constant versus T for R_n = 10. Figure 4b shows the R_n curves in a/h^* = 10; the value of maximum $w(a/2, b/2)$ is 0.000119 mm found at T = 1000 K for R_n = 2. The absolute values of $w(a/2, b/2)$ for R_n = 2 can proceed in higher T = 1000 K of temperature condition.

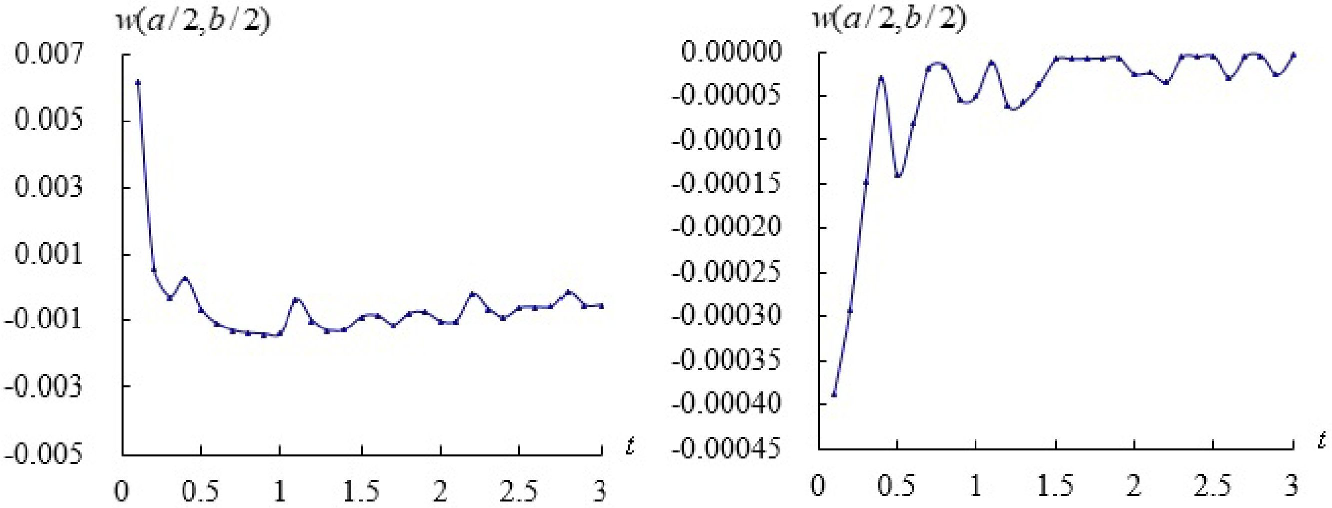

(**a**) (**b**)

Figure 2. $w(a/2, b/2)$ (unit mm) vs. t (unit s): (**a**) for $a/h^* = 5$; (**b**) for $a/h^* = 10$.

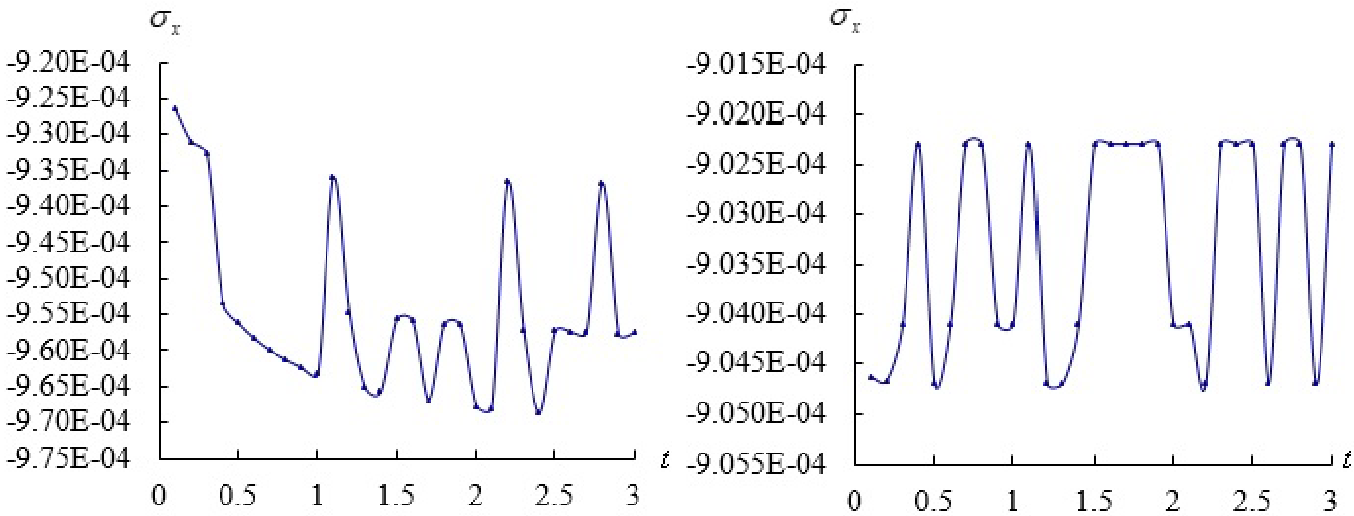

(**a**) (**b**)

Figure 3. Stress σ_x (unit GPa) vs. t (unit s): (**a**) $a/h^* = 5$; (**b**) for $a/h^* = 10$.

Figure 5 shows the dominated stresses σ_x (unit GPa) vs. T (unit K) and R_n at center position of $z = -0.5h^*$ for a/h^* = 5. The values of σ_x for R_n = 0.1 and 0.2 can proceed in higher T = 1000 K of temperature condition. The absolute value of maximum σ_x is -1.001130×10^{-3} GPa found at T = 1000 K for R_n = 0.5 and 1.

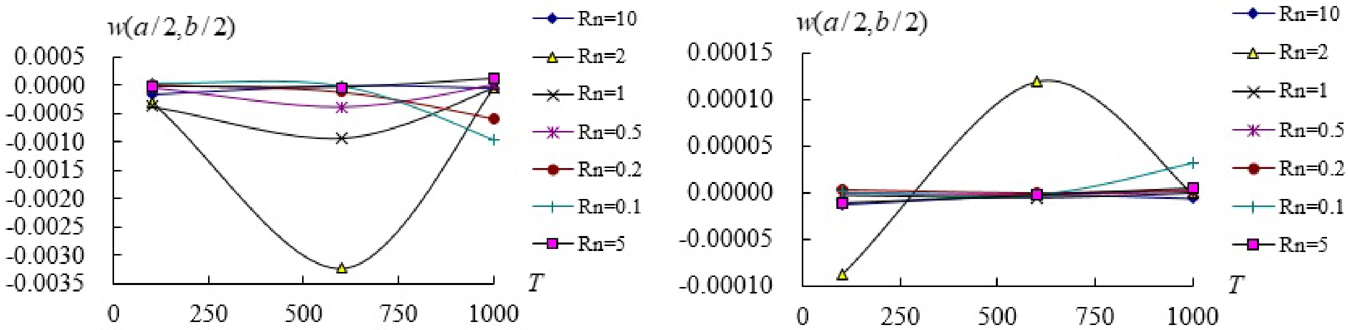

(**a**) (**b**)

Figure 4. $w(a/2, b/2)$ (unit mm) vs. T (unit K): (**a**) for $a/h^* = 5$; (**b**) for $a/h^* = 10$.

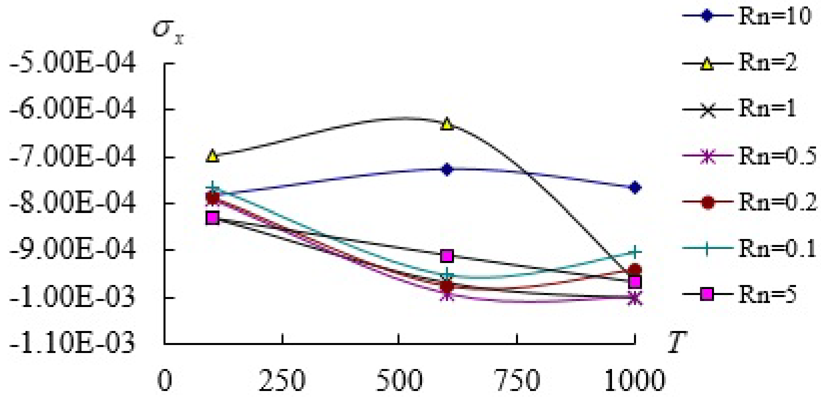

Figure 5. σ_x (unit GPa) vs. T (unit K) for $a/h^* = 5$.

3.4. Transient Responses of Deflection and Stress

The transient responses of $w(a/2, b/2)$ (unit mm) are computed for a/h^* = 10 with fixed ω_{11} = 0.065469/s under c_1 = 0.925925/mm^2, $R_n = 1$, advanced nonlinear $k_\alpha = -3.535402$, T = 600 K and $\overline{T_1}$ = 100 K. Figure 6 shows the transient $w(a/2, b/2)$ compared by using simply homogeneous equation and fully homogeneous equation with γ = 785.3982/s, respectively, for t = 0.001 s–0.025 s. The $w(a/2, b/2)$ amplitudes in the simply homogeneous equation are found in greater values and overestimated in the approach. The explanation provided more clearly for Figure 6. There are two equation types (simply homogeneous equation and fully homogeneous equation) used to calculate the values of ω_{mn} for Equation (6). The simply homogeneous equation and fully homogeneous equation are listed in the Appendix A. Figure 7 also shows the transient $w(a/2, b/2)$ compared with values of nonlinear varied k_α (expression with containing the c_1 factor) and linear varied k_α (expression without containing the c_1 factor) for the a/h^* = 10 case of γ = 785.3982/s. The transient $w(a/2, b/2)$ values in linear varied k_α case are overestimated with respect to the nonlinear varied k_α case.

3.5. Future Works

There is some recent research in the field of FGMs, e.g., in 2023, Sirimontree et al. [19] presented a vibroacoustic study for the sandwich magneto-electro-elastic cylindrical FGM nanoshell in the external flow and under thermal environment. Based on the fundamental study for thermal vibration of thick FGM plates in 2019 by Hong [10], it would be interesting to further study the advanced dynamic vibration of FGM plates/cylindrical shells in supersonic flow.

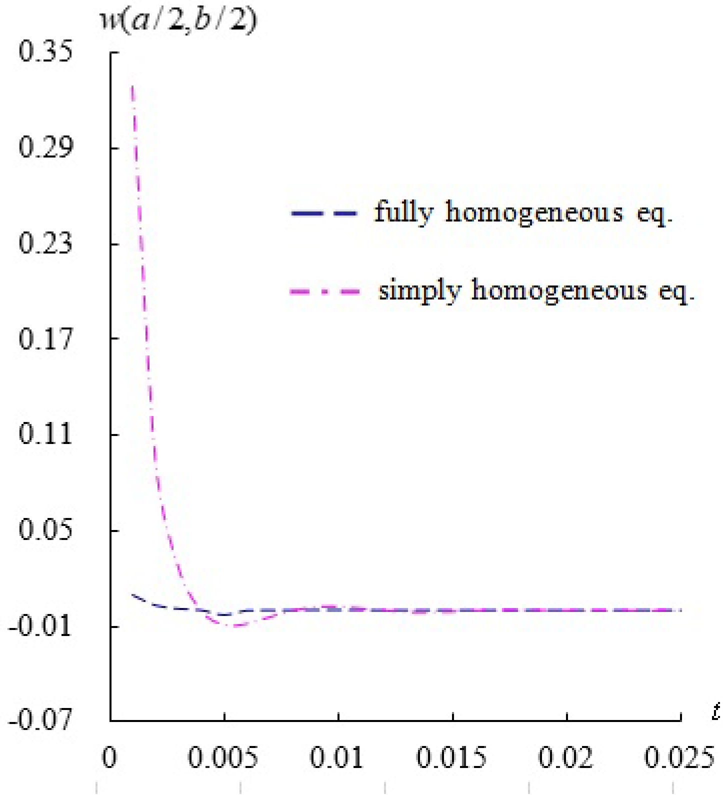

Figure 6. Transient response of $w(a/2, b/2)$ (unit mm) vs. t (unit s) compared with simply and fully homogeneous eq.

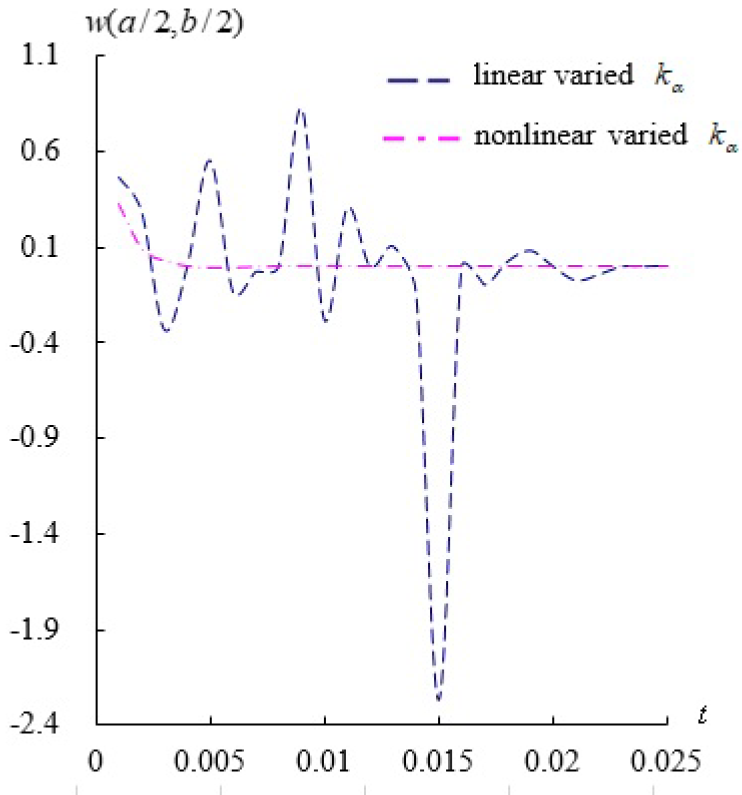

Figure 7. Transient response of $w(a/2, b/2)$ (unit mm) vs. t (unit s) compared with nonlinear and linear varied k_α.

4. Conclusions

The dynamic responses of deflection and stress computed by the GDQ method in TSDT thick FGM plates under sinusoidal applied heat loads by considering the parameter effects of advanced k_α, T and R_n. By using the simply homogeneous equation to calculate the natural frequency. The advanced nonlinear k_α are usually in functions of c_1, R_n and T. The maximum absolute value of $w(a/2, b/2)$ is 0.006138 mm at t = 0.1 s found for a/h^* = 5 with advanced k_α = -3.535402 and γ = 15.707964/s. The $w(a/2, b/2)$ amplitudes in simply homogeneous equation are found in greater values and overestimated in the approach. The transient responses of $w(a/2, b/2)$ are compared with the cases of simply homogeneous equation and fully homogeneous equation. Also, the transient responses of $w(a/2, b/2)$ are compared with the cases of nonlinear and linear varied k_α.

Funding: The funding of this paper is by a grant MOST 111-2221-E-164-001 from National Science and Technology Council (NSTC), Taiwan, ROC.

Institutional Review Board Statement: Not applicable for studies not involving humans or animals.

Informed Consent Statement: Not applicable for studies not involving humans.

Data Availability Statement: The manuscript completely presented the data used to generate the figures and tables. Data are all available on request. All the data are generated by the author; data are openly available.

Conflicts of Interest: The author has declared no conflict of interest. There is no funder for this study. There is only the author stated in the manuscripts.

Appendix A

The boundary equations of displacements and shear rotations with amplitudes: a_{mn}, b_{mn}, c_{mn}, d_{mn}, and e_{mn} for 4-sided simply supported plates are given explicitly as follows,

$$\begin{aligned} u^0(x,y) &= a_{mn}\cos(m\pi x/a)\sin(n\pi y/b) \\ v^0(x,y) &= b_{mn}\sin(m\pi x/a)\cos(n\pi y/b) \\ w(x,y) &= c_{mn}\sin(m\pi x/a)\sin(n\pi y/b) \\ \psi_x(x,y) &= d_{mn}\cos(m\pi x/a)\sin(n\pi y/b) \\ \psi_y(x,y) &= e_{mn}\sin(m\pi x/a)\cos(n\pi y/b) \end{aligned} \tag{A1}$$

The fully homogeneous equation is expressed as follows,

$$\begin{bmatrix} FH_{11} - \frac{I_0\lambda_{mn}}{I_0} & FH_{12} & FH_{13} + \frac{c_1 I_3\left(\frac{m\pi}{a}\right)\lambda_{mn}}{I_0} & FH_{14} - \frac{J_1\lambda_{mn}}{I_0} & FH_{15} \\ FH_{12} & FH_{22} - \frac{I_0\lambda_{mn}}{I_0} & FH_{23} + \frac{c_1 I_3\left(\frac{n\pi}{b}\right)\lambda_{mn}}{I_0} & FH_{24} & FH_{25} - \frac{J_1\lambda_{mn}}{I_0} \\ FH_{13} + \frac{c_1 I_3\left(\frac{m\pi}{a}\right)\lambda_{mn}}{I_0} & FH_{23} + \frac{c_1 I_3\left(\frac{n\pi}{b}\right)\lambda_{mn}}{I_0} & FH_{33} - \left[I_0 + {c_1}^2 I_6\left(\frac{m\pi}{a}\right)^2 + {c_1}^2 I_6\left(\frac{n\pi}{b}\right)^2\right]\lambda_{mn}/I_0 & FH_{34} + \frac{c_1 J_4\left(\frac{m\pi}{a}\right)\lambda_{mn}}{I_0} & FH_{35} + \frac{c_1 J_4\left(\frac{n\pi}{b}\right)\lambda_{mn}}{I_0} \\ FH_{14} - \frac{J_1\lambda_{mn}}{I_0} & FH_{24} & FH_{34} + \frac{c_1 J_4\left(\frac{m\pi}{a}\right)\lambda_{mn}}{I_0} & FH_{44} - \frac{K_2\lambda_{mn}}{I_0} & FH_{45} \\ FH_{15} & FH_{25} - \frac{J_1\lambda_{mn}}{I_0} & FH_{35} + \frac{c_1 J_4\left(\frac{n\pi}{b}\right)\lambda_{mn}}{I_0} & FH_{45} & FH_{55} - \frac{K_2\lambda_{mn}}{I_0} \end{bmatrix} \begin{Bmatrix} a_{mn} \\ b_{mn} \\ c_{mn} \\ d_{mn} \\ e_{mn} \end{Bmatrix} = \begin{Bmatrix} 0 \\ 0 \\ 0 \\ 0 \\ 0 \end{Bmatrix} \tag{A2}$$

where $\lambda_{mn} = I_0{\omega_{mn}}^2$, $I_i = \sum_{k=1}^{N^*} \int_k^{k+1} \rho^{(k)} z^i dz$ (i = 0, 1, 2, ..., 6), $\rho^{(k)}$ is the density of k th constituent ply, $FH_{11} = A_{11}(m\pi/a)^2 + A_{66}(n\pi/b)^2$, etc. all of the parameters and coefficients can be referred [10].

The simply homogeneous equation is expressed as follows,

$$\begin{bmatrix} FH_{11} - \lambda_{mn} & FH_{12} & 0 & 0 & 0 \\ FH_{12} & FH_{22} - \lambda_{mn} & 0 & 0 & 0 \\ 0 & 0 & FH_{33} - \lambda_{mn} & FH_{34} & FH_{35} \\ 0 & 0 & FH_{34} & FH_{44} - \frac{K_2}{I_0}\lambda_{mn} & FH_{45} \\ 0 & 0 & FH_{35} & FH_{45} & FH_{55} - \frac{K_2}{I_0}\lambda_{mn} \end{bmatrix} \begin{Bmatrix} a_{mn} \\ b_{mn} \\ c_{mn} \\ d_{mn} \\ e_{mn} \end{Bmatrix} = \begin{Bmatrix} 0 \\ 0 \\ 0 \\ 0 \\ 0 \end{Bmatrix} \tag{A3}$$

The typical ω_{mn} (unit 1/s) vs. mode shapes m and n (from 1 to 9) of the vibrating plate are reported in the Table A1 under nonlinear varied k_α, c_1, $R_n = 0.5$ and T = 300 K.

Table A1. ω_{mn} vs. m and n under nonlinear varied k_α, c_1, $R_n = 0.5$ and T = 300 K.

a/h^*	ω_{1n} (unit 1/s)								
	$n=1$	$n=2$	$n=3$	$n=4$	$n=5$	$n=6$	$n=7$	$n=8$	$n=9$
5	0.030248	0.012079	0.010355	0.005455	0.003399	0.007451	0.006401	0.005629	0.005048
10	0.060513	0.042673	0.035361	0.020371	0.015934	0.031821	0.014847	0.011815	0.006108
a/h^*	ω_{2n} (unit 1/s)								
	$n=1$	$n=2$	$n=3$	$n=4$	$n=5$	$n=6$	$n=7$	$n=8$	$n=9$
5	0.019082	0.009523	0.010442	0.004176	0.007139	0.007156	0.006237	0.005555	0.005061
10	0.023112	0.030248	0.014602	0.012079	0.015355	0.010355	0.015735	0.005455	0.006460
a/h^*	ω_{3n} (unit 1/s)								
	$n=1$	$n=2$	$n=3$	$n=4$	$n=5$	$n=6$	$n=7$	$n=8$	$n=9$
5	0.008481	0.007713	0.010970	0.009022	0.007734	0.006781	0.006089	0.006744	0.001734
10	0.027054	0.023712	0.012403	0.016924	0.009628	0.011476	0.015462	0.004309	0.006783
a/h^*	ω_{4n} (unit 1/s)								
	$n=1$	$n=2$	$n=3$	$n=4$	$n=5$	$n=6$	$n=7$	$n=8$	$n=9$
5	0.010463	0.009661	0.008689	0.007765	0.007011	0.006711	0.002147	0.001856	0.001620
10	0.012677	0.019082	0.010558	0.009523	0.012944	0.010442	0.013141	0.004176	0.007080
a/h^*	ω_{5n} (unit 1/s)								
	$n=1$	$n=2$	$n=3$	$n=4$	$n=5$	$n=6$	$n=7$	$n=8$	$n=9$
5	0.005210	0.007929	0.007340	0.006738	0.006999	0.002301	0.001972	0.001712	0.001502
10	0.010366	0.015779	0.014532	0.008480	0.008050	0.017151	0.011124	0.004087	0.008826
a/h^*	ω_{6n} (unit 1/s)								
	$n=1$	$n=2$	$n=3$	$n=4$	$n=5$	$n=6$	$n=7$	$n=8$	$n=9$
5	0.006944	0.006693	0.006307	0.005852	0.005405	0.004941	0.004526	0.004152	0.003821
10	0.008856	0.008481	0.008063	0.007713	0.008185	0.010970	0.009856	0.009022	0.003542
a/h^*	ω_{7n} (unit 1/s)								
	$n=1$	$n=2$	$n=3$	$n=4$	$n=5$	$n=6$	$n=7$	$n=8$	$n=9$
5	0.005915	0.005753	0.005469	0.005921	0.005027	0.004625	0.004279	0.003964	0.003679
10	0.012552	0.008211	0.011614	0.010954	0.010263	0.009585	0.006448	0.008361	0.007834
a/h^*	ω_{8n} (unit 1/s)								
	$n=1$	$n=2$	$n=3$	$n=4$	$n=5$	$n=6$	$n=7$	$n=8$	$n=9$
5	0.005130	0.005009	0.006575	0.005036	0.004590	0.004284	0.004006	0.003746	0.003506
10	0.010707	0.010463	0.010102	0.009661	0.009180	0.008689	0.004282	0.007765	0.007361
a/h^*	ω_{9n} (unit 1/s)								
	$n=1$	$n=2$	$n=3$	$n=4$	$n=5$	$n=6$	$n=7$	$n=8$	$n=9$
5	0.004509	0.007183	0.005173	0.004502	0.004205	0.003967	0.003743	0.003530	0.003328
10	0.005754	0.005626	0.005439	0.005199	0.004907	0.007963	0.007584	0.007228	0.006915

References

1. Zenkour, A.M.; El-Shahrany, H.D. Vibration suppression of advanced plates embedded magnetostrictive layers via various theories. *J. Mater. Res. Technol.* **2020**, *9*, 4727–4748. [CrossRef]
2. Wu, D.; Lin, L.; Ren, H. Thermal/vibration joint experimental investigation on lightweight ceramic insulating material for hypersonic vehicles in extremely high-temperature environment up to 1500 °C. *Ceram. Int.* **2020**, *46*, 14439–14447. [CrossRef]
3. Shariyat, M.; Mohammadjani, R. 3D nonlinear variable strain-rate-dependent-order fractional thermoviscoelastic dynamic stress investigation and vibration of thick transversely graded rotating annular plates/discs. *Appl. Math. Model.* **2020**, *84*, 287–323. [CrossRef]
4. Fan, Z.; Liu, Y.; Chen, X.; Jiang, Y.; Zhang, S.; Wang, Y. Research on fatigue of TSV-Cu under thermal and vibration coupled bade on numerical analysis. *Microelectron. Reliab.* **2020**, *106*, 113590. [CrossRef]
5. Su, Z.; Wang, L.; Sun, K.; Wang, D. Vibration characteristic and flutter analysis of electrically restrained stiffened functionally graded plates in thermal environment. *Int. J. Mech. Sci.* **2019**, *157–158*, 872–884. [CrossRef]
6. Fang, J.; Gu, J.; Wang, H.; Zhang, X. Thermal effect on vibrational behaviors of rotating functionally graded microbeams. *Eur. J. Mech. A/Solids* **2019**, *75*, 497–515. [CrossRef]
7. Duc, N.D.; Cong, P.H.; Quang, V.D. Nonlinear dynamic and vibration analysis of piezoelectric eccentrically stiffened FGM plates in thermal environment. *Int. J. Mech. Sci.* **2016**, *115–116*, 711–722. [CrossRef]
8. Huang, X.L.; Shen, H.S. Vibration and dynamic response of functionally graded plates with piezoelectric actuators in thermal environments. *J. Sound Vib.* **2006**, *289*, 25–53. [CrossRef]
9. Huang, X.L.; Shen, H.S. Nonlinear vibration and dynamic response of functionally graded plates in thermal environments. *Int. J. Solids Struct.* **2004**, *41*, 2403–2427. [CrossRef]
10. Hong, C.C. GDQ computation for thermal vibration of thick FGM plates by using fully homogeneous equation and TSDT. *Thin-Walled Struct.* **2019**, *135*, 78–88. [CrossRef]
11. Hong, C.C. Thermal vibration and transient response of magnetostrictive functionally graded material plates. *Eur. J. Mech. A/Solids* **2014**, *43*, 78–88. [CrossRef]
12. Hong, C.C. Rapid heating induced vibration of magnetostrictive functionally graded material plates. *Trans. ASME J. Vib. Acoust.* **2012**, *134*, 021019. [CrossRef]
13. Lee, S.J.; Reddy, J.N.; Rostam-Abadi, F. Transient analysis of laminated composite plates with embedded smart-material layers. *Finite Elem. Anal. Des.* **2004**, *40*, 463–483. [CrossRef]
14. Reddy, J.N. *Energy Principles and Variational Methods in Applied Mechanics*; Wiley: New York, NY, USA, 2002.
15. Hong, C.C. Thermal vibration of magnetostrictive material in laminated plates by the GDQ method. *Open Mech. J.* **2007**, *1*, 29–37. [CrossRef]
16. Bert, C.W.; Jang, S.K.; Striz, A.G. Nonlinear bending analysis of orthotropic rectangular plates by the method of differential quadrature. *Comput. Mech.* **1989**, *5*, 217–226. [CrossRef]
17. Shu, C.; Du, H. Implementation of clamped and simply supported boundary conditions in the GDQ free vibration analyses of beams and plates. *Int. J. Solids Struct.* **1997**, *34*, 819–835. [CrossRef]
18. Hong, C.C. Advanced frequency analysis of thick FGM plates using third-order shear deformation theory with a nonlinear shear correction coefficient. *J. Struct. Eng. Appl. Mech.* **2022**, *5*, 143–160. [CrossRef]
19. Sirimontree, S.; Thongchom, C.; Saffari, P.R.; Refahati, N.; Saffari, P.R.; Jearsiripongkul, T.; Keawsawasvong, S. Effects of thermal environment and external mean flow on sound transmission loss of sandwich functionally graded magneto-electro-elastic cylindrical nanoshell. *Eur. J. Mech. A/Solids* **2023**, *97*, 104774. [CrossRef]